

Multi-strategy structural damage detection based on included angle of vectors and sparse regularization

Huanlin Liu^a, Ling Yu^{*}, Ziwei Luo^a and Zexiang Chen^b

MOE Key Laboratory of Disaster Forecast and Control in Engineering,
School of Mechanics and Construction Engineering, Jinan University, Guangzhou 510632, China

(Received February 27, 2020, Revised May 29, 2020, Accepted May 30, 2020)

Abstract. Recently, many structural damage detection (SDD) methods have been proposed to monitor the safety of structures. As an important modal parameter, mode shape has been widely used in SDD, and the difference of vectors was adopted based on sensitivity analysis and mode shapes in the existing studies. However, amplitudes of mode shapes in different measured points are relative values. Therefore, the difference of mode shapes will be influenced by their amplitudes, and the SDD results may be inaccurate. Focus on this deficiency, a multi-strategy SDD method is proposed based on the included angle of vectors and sparse regularization in this study. Firstly, inspired by modal assurance criterion (MAC), a relationship between mode shapes and changes in damage coefficients is established based on the included angle of vectors. Then, frequencies are introduced for multi-strategy SDD by a weighted coefficient. Meanwhile, sparse regularization is applied to improve the ill-posedness of the SDD problem. As a result, a novel convex optimization problem is proposed for effective SDD. To evaluate the effectiveness of the proposed method, numerical simulations in a planar truss and experimental studies in a six-story aluminum alloy frame in laboratory are conducted. The identified results indicate that the proposed method can effectively reduce the influence of noises, and it has good ability in locating structural damages and quantifying damage degrees.

Keywords: structural damage detection (SDD); multi-strategy method; sparse regularization; included angle of vectors

1. Introduction

As an indirect technique and one crucial step in the field of structural health monitoring (SHM), structural damage detection (SDD) aims at monitoring the safety of structures from structural responses. Many SDD methods have been proposed in recent years (Yan *et al.* 2007, Fan and Qiao 2011, Li and Chen 2013, Moughty and Casas 2017, Alkayem *et al.* 2018).

Features sensitive to structural damages should be extracted from structural responses so that effective SDD can be achieved under the influence of noises. Some dynamic characteristics, such as frequency, mode shape, frequency response function (FRF), modal strain energy (Shi *et al.* 1998) and transmissibility function (Zhou and Wahab 2017, Yan *et al.* 2019) have been taken as features, and objective functions related to these dynamic characteristics have been proposed by scholars in the existing studies. For example, Cawley and Adams (1979) firstly proposed a frequency-based method for SDD. It is effective to extract frequencies from structural responses in the frequency domain, and changes in frequencies are sensitive to structural damages. However, frequencies are global parameters related to structural damages, so multiple SDD results may be obtained from the same changes in

frequencies. To overcome this drawback, mode shapes were introduced into SDD because they can reflect the influence of local damages (Pandey *et al.* 1991, Ratcliffe 1997). When excitations and structural responses are known, FRFs can be used for SDD (Lee and Shin 2002, Huang *et al.* 2012). Other dynamic characteristics and their modified methods have been proposed by some scholars (Li *et al.* 2017, Bagherahmadi and Seyedpoor 2018, Liu *et al.* 2018, Vahidi *et al.* 2019, Chang *et al.* 2019).

On the other hand, due to the ill-posedness of SDD problem, although many methods have been proposed, the identified results may be inaccurate under the influence of noises. Thus, many regularization techniques have been introduced to improve the SDD results (Friswell 2007), such as Tikhonov regularization, sparse regularization and so on.

The Tikhonov regularization is the most common regularization technique, and the l_2 -norm is used to improve the ill-posedness of SDD problem. However, the solutions obtained from Tikhonov regularization are dense, which are not consistent with the sparsity of structural damages.

Recently, by utilizing the sparsity of structural damages, sparse regularization was introduced into SDD. For example, Zhou *et al.* (2015) combined the l_1 -norm regularization with frequencies based on sensitivity analysis to improve the SDD results. Then, Hou *et al.* (2018) utilized both frequencies and mode shapes with the l_1 -norm regularization for SDD. Because the l_1 -norm regularization improves the ill-posedness of SDD problem by using the l_1 -norm, sparse solutions can be obtained under the restricted conditions. Moreover, comparative studies between

*Corresponding author, Ph.D., Professor
E-mail: lyu1997@163.com

^a Ph.D. Student

^b M.Sc. Student

Tikhonov regularization and sparse regularization have been investigated by Zhang and Xu (2016). These existing studies indicate that the sparse regularization is more reasonable to improve the SDD results compared with Tikhonov regularization.

Among these methods, finite element (FE) model-based SDD methods have advantages to simultaneously locate structural damages and quantify damage degrees, and modal parameters have been widely applied because they can be easily obtained from the global mass and stiffness of a structure (Zhou *et al.* 2015, Hou *et al.* 2018). Based on sensitivity analysis, the relationship between the difference of modal parameters and changes in damage coefficients was given between the real structure and corresponding FE model (Zhao and DeWolf 1999). However, the amplitudes of mode shapes in different measured points are relative values, so the scaling of mode shapes respectively obtained from the structural responses and the FE model may have great difference, which will affect the identified accuracy.

Rather than difference of mode shapes, the included angle of mode shapes is considered in this paper. Therefore, inspired by modal assurance criterion (MAC) (Allemang 2003), a novel relationship between modal parameters and changes in damage coefficients is defined. Meanwhile, to reasonably evaluate the influences of noises, frequencies are also introduced by a weighted coefficient so that multi-strategy SDD is achieved. Moreover, the l_1 -norm regularization is introduced to reasonably improve the identified accuracy. As a result, a novel convex optimization problem is proposed in this study and the SDD results are obtained by solving this problem with a fast iterative shrinkage-thresholding algorithm (FISTA) (Beck and Teboulle 2009).

This paper is organized as follows: The basic theories of the proposed multi-strategy SDD method are introduced in Section 2. Then, some numerical validations of the proposed method are conducted in a 31-bar planar truss in Section 3. Moreover, experimental studies in a six-story aluminum alloy frame are conducted in Section 4. Finally, several conclusions are summarized in Section 5.

2. Basic theories

2.1 Sensitivity analysis

In this paper, a n -degree of freedom (DOF) FE model is used to describe the real structure (Esfandiari *et al.* 2018). The equilibrium equation for the undamped structural vibration system can be expressed as follows:

$$(\mathbf{K} - 4\pi^2 f_i^2 \mathbf{M}) \Phi_i = \mathbf{0} \quad (i=1, 2, \dots, n) \quad (1)$$

where, \mathbf{K} and \mathbf{M} are global stiffness and mass matrices, respectively, Φ_i is the i th mode shape corresponding to the i th frequency f_i .

The global stiffness matrix can be expressed by the element stiffness matrices (Cawley and Adams 1979):

$$\mathbf{K} = \sum_{i=1}^{ne} \alpha_i \mathbf{K}_i \quad (0 \leq \alpha_i \leq 1) \quad (2)$$

where, \mathbf{K}_i is the i th element stiffness matrix, ne is the element number of FE model, α_i is the i th damage coefficient, $\alpha_i = 1$ represents the i th element without damage, $\alpha_i = 0$ represents the i th element is complete failure.

When structural damages occur, only changes in the stiffness of structure are considered. Thus, the sensitivity coefficients of the i th frequency and mode shape with respect to α_j can be respectively obtained:

$$\frac{\partial f_i}{\partial \alpha_j} = \frac{\Phi_i^T \mathbf{K}_j \Phi_i}{8\pi^2 f_i \Phi_i^T \mathbf{M} \Phi_i} \quad (3)$$

$$\frac{\partial \Phi_i}{\partial \alpha_j} = \sum_{s=1, s \neq i}^n \frac{\Phi_s^T \mathbf{K}_j \Phi_i}{4\pi^2 f_i^2 \Phi_s^T \mathbf{M} \Phi_s - \Phi_s^T \mathbf{K} \Phi_s} \Phi_s \quad (4)$$

The differences of the i th frequencies and mode shapes in healthy and damaged states can be approximately expressed respectively by using Eqs. (3) and (4):

$$\frac{\Delta f_i}{\Delta \alpha_j} \approx \frac{\partial f_i}{\partial \alpha_j} \quad (5)$$

$$\frac{\Delta \Phi_i}{\Delta \alpha_j} \approx \frac{\partial \Phi_i}{\partial \alpha_j} \quad (6)$$

where, $\Delta f_i, \Delta \Phi_i$ and $\Delta \alpha_j$ are the difference between the i th frequencies, between the i th mode shapes, and between the j th damage coefficients in healthy and damaged structures, respectively.

The i th mode shape of real structure in damaged state is represented by Φ_i^{RE} , and the i th mode shape of FE model in healthy state is represented by Φ_i^{FE} .

It should be noted that the amplitudes of mode shapes in different measured points are relative values, which are needed to be considered when difference of mode shapes in Eq. (6) is used, so mode shapes in FE model and real structure should be adjusted at first.

To simply illustrate the influence of the amplitudes of mode shapes, a 2-DOF spring-mass system is taken as an example, as shown in Fig. 1. The mass and stiffness in each DOF are 100 kg and 150 kN/m, respectively. Thus, mode shapes of this system can be calculated, which are deemed as mode shapes of FE model in healthy state. Then, it is assumed that the value at k_2 reduces by 80%, the corresponding mode shapes are also obtained, which are deemed as mode shapes of real structure in damaged state.

If mode shapes in these two states are adjusted as mass normalized mode shapes, the difference of mode shapes can be directly used for SDD by sensitivity analysis. The values of the first mode shapes in these two states are $\Phi_1^{\text{FE}} = (0.0526, 0.0851)$ and $\Phi_1^{\text{RE}} = (0.0189, 0.0982)$, respectively. Each mode shape in this spring-mass system can be represented by a plane vector, which can be seen in Fig. 2.

However, mode shapes in real structure may not be adjusted as mass normalized mode shapes, so some modal scale factors are used to adjust the mode shapes in FE model or real structure.

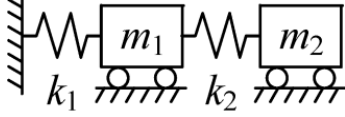


Fig. 1 Two-DOF spring-mass system

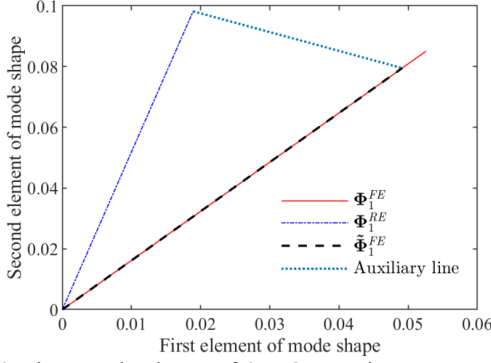


Fig. 2 First mode shape of 2-DOF spring-mass system in different states

For example, Hou *et al.* (2018) gave a modal scale factor for mode shapes, which can be expressed as follows:

$$MSF(\Phi_i^{FE}, \Phi_i^{RE}) = \frac{(\Phi_i^{FE})^T \Phi_i^{RE}}{(\Phi_i^{FE})^T \Phi_i^{FE}} \quad (7)$$

This modal scale factor is applied to the mode shapes in the FE model. For the first mode shape in the 2-DOF stiffness-mass system, the vector Φ_1^{FE} is adjusted as:

$$\tilde{\Phi}_1^{FE} = MSF(\Phi_1^{FE}, \Phi_1^{RE}) \Phi_1^{FE} \quad (8)$$

As a result, the vector $\tilde{\Phi}_1^{FE}$ is equal to (0.0491, 0.0795), which can also be seen in Fig. 2.

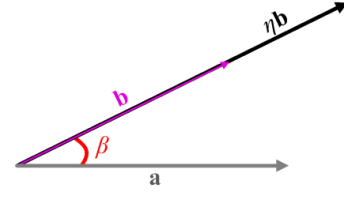
Compared Φ_1^{FE} with $\tilde{\Phi}_1^{FE}$, it can be found that the amplitude of $\tilde{\Phi}_1^{FE}$ is smaller than that of Φ_1^{FE} . The vector Φ_1^{RE} is perpendicular to the auxiliary line, so the function of Eqs. (7) and (8) is to make the projection of $\tilde{\Phi}_1^{FE}$ on Φ_1^{RE} equal to Φ_1^{RE} . Both Φ_1^{FE} and Φ_1^{RE} are mass normalized mode shapes, which are adjusted by same methods and can be directly used in Eq. (6). However, the vector $\tilde{\Phi}_1^{FE}$ is not equal to the vector Φ_1^{FE} . It indicates that the modal scale factor (Hou *et al.* 2018) given in Eq. (7) is not suitable to eliminate the influence brought by the amplitudes of vectors even if the mode shapes are noise-free.

On the other hand, when noise is considered in Φ_1^{RE} , even if same methods are applied to Φ_1^{FE} and Φ_1^{RE} , the modal scale factors will be influenced by noises in Φ_1^{RE} .

Thus, the SDD results may be completely incorrect when the difference of mode shapes in FE model and real structure is used.

2.2 Novel function based on included angle of vectors

Rather than considering the difference of mode shapes in FE model and real structure, MAC (Allemang 2003)

Fig. 3 Geometric representations of vectors \mathbf{a} , \mathbf{b} and $\eta\mathbf{b}$

evaluates these two mode shapes by calculating their normalized scalar product. As shown in Fig. 3, it is assumed that plane vectors \mathbf{b} and $\eta\mathbf{b}$ have different modal scale factors. The included angle between plane vectors \mathbf{a} and \mathbf{b} is represented as β . Similarly, the included angle between vectors \mathbf{a} and $\eta\mathbf{b}$ is also β .

Based on the definition of MAC, the following expressions can be found:

$$MAC(\mathbf{a}, \mathbf{b}) = \frac{|\mathbf{a}^T \mathbf{b}|^2}{(\mathbf{a}^T \mathbf{a})(\mathbf{b}^T \mathbf{b})} = \cos^2 \beta \quad (9)$$

$$MAC(\mathbf{a}, \eta\mathbf{b}) = \frac{|\mathbf{a}^T (\eta\mathbf{b})|^2}{(\mathbf{a}^T \mathbf{a})[(\eta\mathbf{b})^T (\eta\mathbf{b})]} = \cos^2 \beta \quad (10)$$

From Eqs. (9) and (10), it indicates that the values of MAC are not influenced by modal scale factors because the included angle of vectors β is used to evaluate vectors \mathbf{a} and \mathbf{b} or \mathbf{a} and $\eta\mathbf{b}$.

In real engineering, the measured points used for structural responses are limited. In this paper, it is assumed that the number of measured points is n_{mea} , and the vector φ_i is used to represent the measured i th mode shape.

Although MAC can eliminate the influence of modal scale factors, it does not give the direct relationship between mode shapes and changes in damage coefficients. Thus, rather than MAC, to establish the relationship between mode shapes and changes in damage coefficients, the function is defined based on sensitivity analysis, as follows:

$$g_m(\Delta\alpha) = \sum_{i=1}^{n_m} \left[\|\varphi_i^{RE}\|_2^2 \|\varphi_i^{FE} - \mathbf{S}_i^m \Delta\alpha\|_2^2 - \left\| (\varphi_i^{RE})^T (\varphi_i^{FE} - \mathbf{S}_i^m \Delta\alpha) \right\|_2^2 \right] \quad (11)$$

where, $\mathbf{S}_i^m = \begin{bmatrix} \frac{\partial \varphi_i}{\partial \alpha_1} & \frac{\partial \varphi_i}{\partial \alpha_2} & \dots & \frac{\partial \varphi_i}{\partial \alpha_{ne}} \end{bmatrix}$, n_m is the order number of mode shapes, $\Delta\alpha = [\Delta\alpha_1 \ \Delta\alpha_2 \ \dots \ \Delta\alpha_{ne}]$.

It should be pointed out that $g_m(\Delta\alpha) \geq 0$ because

$$\|\varphi_i^{RE}\|_2^2 \|\varphi_i^{FE} - \mathbf{S}_i^m \Delta\alpha\|_2^2 \geq \left\| (\varphi_i^{RE})^T (\varphi_i^{FE} - \mathbf{S}_i^m \Delta\alpha) \right\|_2^2.$$

Eq. (11) is a convex function because $\forall \theta_1, \theta_2$ in the definition of domain of $\Delta\alpha$ and $\forall t \in [0, 1]$:

$$\begin{aligned} & g_m[t\theta_1 + (1-t)\theta_2] - t g_m(\theta_1) - (1-t) g_m(\theta_2) \\ &= \sum_{i=1}^{n_m} \left\{ -t(1-t) \left[\|\varphi_i^{RE}\|_2^2 \|\mathbf{S}_i^m(\theta_1 - \theta_2)\|_2^2 - \left\| (\varphi_i^{RE})^T \mathbf{S}_i^m(\theta_1 - \theta_2) \right\|_2^2 \right] \right\} \leq 0 \end{aligned} \quad (12)$$

For the plane vectors \mathbf{a} and \mathbf{b} , it can be found that $\|\mathbf{a}\|_2^2 \|\mathbf{b}\|_2^2 - \|\mathbf{a}^T \mathbf{b}\|_2^2 = \|\mathbf{a}\|_2^2 \|\mathbf{b}\|_2^2 (1 - \cos^2 \beta)$. At the same time, for the plane vectors \mathbf{a} and $\eta \mathbf{b}$, it has $\|\mathbf{a}\|_2^2 \|\eta \mathbf{b}\|_2^2 - \|\mathbf{a}^T (\eta \mathbf{b})\|_2^2 = \|\mathbf{a}\|_2^2 \|\eta \mathbf{b}\|_2^2 (1 - \cos^2 \beta)$. Although the amplitudes of vectors in these two equations are taken into account, both of these two equations evaluate two vectors by the term $(1 - \cos^2 \beta)$. That is to say, rather than the difference of mode shapes, the included angle of mode shapes is evaluated by Eq. (11).

2.3 Multi-strategy SDD with sparse regularization

Both frequencies and mode shapes are important modal parameters which are sensitivity to structural damages and can be effectively obtained from structural responses. In real structure, structural responses are inevitably influenced by noises. In this case, noisy frequencies and mode shapes can reflect the structural damages in different perspectives. Thus, it is suitable to use both frequencies and mode shapes for SDD. According to Eqs. (3) and (5), the following function of frequencies is defined:

$$g_f(\Delta \boldsymbol{\alpha}) = \sum_{i=1}^{n_f} \left[\mathbf{S}_i^f \Delta \boldsymbol{\alpha} - (f_i^{FE} - f_i^{RE}) \right]^2 / (f_i^{FE})^2 \quad (13)$$

$$= \|\mathbf{S}^f \Delta \boldsymbol{\alpha} - \Delta \mathbf{f}\|_2^2$$

where, $\mathbf{S}_i^f = \begin{bmatrix} \frac{\partial f_i}{\partial \alpha_1} & \frac{\partial f_i}{\partial \alpha_2} & \cdots & \frac{\partial f_i}{\partial \alpha_{n_e}} \end{bmatrix}$, n_f is the order number of frequencies, f_i^{FE} and f_i^{RE} are the i th frequencies of FE model in healthy state and real structure in damaged state, respectively.

Eq. (13) is also a convex function because $\forall \boldsymbol{\theta}_1, \boldsymbol{\theta}_2$ in the definition of domain of $\Delta \boldsymbol{\alpha}$ and $\forall t \in [0, 1]$:

$$g_f \left[t \boldsymbol{\theta}_1 + (1-t) \boldsymbol{\theta}_2 \right] - t g_f(\boldsymbol{\theta}_1) - (1-t) g_f(\boldsymbol{\theta}_2) = -t(1-t) \|\mathbf{S}^f(\boldsymbol{\theta}_1 - \boldsymbol{\theta}_2)\|_2^2 \leq 0 \quad (14)$$

Because the magnitudes of vectors are considered in Eq. (11), to use both frequencies and mode shapes for SDD, a novel objective function can be obtained from Eqs. (11) and (13) by using a weighted coefficient γ ($\gamma > 0$):

$$g(\Delta \boldsymbol{\alpha}) = \|\mathbf{S}^f \Delta \boldsymbol{\alpha} - \Delta \mathbf{f}\|_2^2 + \gamma \sum_{i=1}^{n_m} \left[\|\boldsymbol{\varphi}_i^{RE}\|_2^2 \|\boldsymbol{\varphi}_i^{FE} - \mathbf{S}_i^m \Delta \boldsymbol{\alpha}\|_2^2 - \left\| (\boldsymbol{\varphi}_i^{RE})^T (\boldsymbol{\varphi}_i^{FE} - \mathbf{S}_i^m \Delta \boldsymbol{\alpha}) \right\|_2^2 \right] \quad (15)$$

Because approximate relationships in Eqs. (5) and (6) are used, and noisy frequencies and mode shapes are considered, the vector $\Delta \boldsymbol{\alpha}$ identified from Eq. (15) is inaccurate. Herein, by considering the sparsity of vector $\Delta \boldsymbol{\alpha}$, the l_1 -norm regularization (Zhou *et al.* 2015, Hou *et al.* 2018) is introduced to improve the identification accuracy. Therefore, a convex optimization problem for SDD is given as follows:

$$\Delta \boldsymbol{\alpha} = \min_{\Delta \boldsymbol{\alpha} \in \mathbb{R}^{n_e}} \left\{ \|\mathbf{S}^f \Delta \boldsymbol{\alpha} - \Delta \mathbf{f}\|_2^2 + \gamma \sum_{i=1}^{n_m} \left[\|\boldsymbol{\varphi}_i^{RE}\|_2^2 \|\boldsymbol{\varphi}_i^{FE} - \mathbf{S}_i^m \Delta \boldsymbol{\alpha}\|_2^2 - \left\| (\boldsymbol{\varphi}_i^{RE})^T (\boldsymbol{\varphi}_i^{FE} - \mathbf{S}_i^m \Delta \boldsymbol{\alpha}) \right\|_2^2 \right] + \lambda \|\Delta \boldsymbol{\alpha}\|_1 \right\} \quad (16)$$

where, $\lambda > 0$ is the regularization parameter.

In this paper, the convex optimization problem in Eq. (16) is solved by FISTA, and several preprocessing should be conducted as follows (Beck and Teboulle 2009).

The gradient of the convex function in Eq. (15) should be given at first:

$$\begin{aligned} \nabla g &= 2(\mathbf{S}^f)^T \mathbf{S}^f \Delta \boldsymbol{\alpha} - 2(\mathbf{S}^f)^T \Delta \mathbf{f} + \\ &\gamma \sum_{i=1}^{n_m} \left[2(\boldsymbol{\varphi}_i^{RE})^T \boldsymbol{\varphi}_i^{RE} (\mathbf{S}_i^m)^T \mathbf{S}_i^m \Delta \boldsymbol{\alpha} - \right. \\ &2(\mathbf{S}_i^m)^T \boldsymbol{\varphi}_i^{RE} (\boldsymbol{\varphi}_i^{RE})^T \mathbf{S}_i^m \Delta \boldsymbol{\alpha} - \\ &2(\boldsymbol{\varphi}_i^{RE})^T \boldsymbol{\varphi}_i^{RE} (\mathbf{S}_i^m)^T \boldsymbol{\varphi}_i^{FE} + \\ &\left. 2(\boldsymbol{\varphi}_i^{RE})^T \boldsymbol{\varphi}_i^{FE} (\mathbf{S}_i^m)^T \boldsymbol{\varphi}_i^{RE} \right] \\ &= \mathbf{G} \Delta \boldsymbol{\alpha} - \mathbf{c} \end{aligned} \quad (17)$$

where, the symbols “ \mathbf{G} ” and “ \mathbf{c} ” in Eq. (17) are used to simply represent the gradient expression, i.e.,

$$\mathbf{G} = 2(\mathbf{S}^f)^T \mathbf{S}^f + \gamma \sum_{i=1}^{n_m} \left[2(\boldsymbol{\varphi}_i^{RE})^T \boldsymbol{\varphi}_i^{RE} (\mathbf{S}_i^m)^T \mathbf{S}_i^m - 2(\mathbf{S}_i^m)^T \boldsymbol{\varphi}_i^{RE} (\boldsymbol{\varphi}_i^{RE})^T \mathbf{S}_i^m \right]$$

and

$$\mathbf{c} = 2(\mathbf{S}^f)^T \Delta \mathbf{f} + \gamma \sum_{i=1}^{n_m} \left[2(\boldsymbol{\varphi}_i^{RE})^T \boldsymbol{\varphi}_i^{RE} (\mathbf{S}_i^m)^T \boldsymbol{\varphi}_i^{FE} - 2(\boldsymbol{\varphi}_i^{RE})^T \boldsymbol{\varphi}_i^{FE} (\mathbf{S}_i^m)^T \boldsymbol{\varphi}_i^{RE} \right]$$

Then, the (smallest) Lipschitz constant of the gradient ∇g can be obtained:

$$\begin{aligned} L(g) &= 2\lambda_{\max} \left\{ 2(\mathbf{S}^f)^T \mathbf{S}^f \Delta \boldsymbol{\alpha} + \right. \\ &\gamma \sum_{i=1}^{n_m} \left[2(\boldsymbol{\varphi}_i^{RE})^T \boldsymbol{\varphi}_i^{RE} (\mathbf{S}_i^m)^T \mathbf{S}_i^m - \right. \\ &\left. 2(\mathbf{S}_i^m)^T \boldsymbol{\varphi}_i^{RE} (\boldsymbol{\varphi}_i^{RE})^T \mathbf{S}_i^m \right] \left. \right\} \\ &= 2\lambda_{\max}(\mathbf{G}) \end{aligned} \quad (18)$$

where, $\lambda_{\max}(\bullet)$ is the maximum eigenvalue of \mathbf{G} .

As a result, the FISTA with constant step size is applied to solve Eq. (16), which can be seen in Fig. 4. The maximum number of iterations is taken as 1×10^4 , which is taken as the stop criterion of FISTA.

Because the value of regularization parameter λ will affect SDD results obviously, a near-optimal regularization parameter λ_{opt} should be given to obtain reasonable results. Some regularization parameters are given at first. Then, inspired by the Akaike information criterion (AIC) (Liddle 2007), the parameter λ_{opt} is chosen based on the following equation:

$$\begin{aligned} \lambda_{opt} &= \min_{\lambda} \left\{ \frac{1}{1+\gamma} n_f \ln \left(\|\mathbf{S}^f \Delta \boldsymbol{\alpha}(\lambda) - \Delta \mathbf{f}\|_2^2 / n_f \right) + \right. \\ &\frac{\gamma}{1+\gamma} n_{mea} \sum_{i=1}^{n_m} \ln \left[\|\boldsymbol{\varphi}_i^{RE}\|_2^2 \|\boldsymbol{\varphi}_i^{FE} - \mathbf{S}_i^m \Delta \boldsymbol{\alpha}(\lambda)\|_2^2 / n_{mea} - \right. \\ &\left. \left\| (\boldsymbol{\varphi}_i^{RE})^T (\boldsymbol{\varphi}_i^{FE} - \mathbf{S}_i^m \Delta \boldsymbol{\alpha}(\lambda)) \right\|_2^2 / n_{mea} \right] + 4k_{\Delta \boldsymbol{\alpha}(\lambda)} \left. \right\} \end{aligned} \quad (19)$$

where, $k_{\Delta \boldsymbol{\alpha}(\lambda)}$ is the sparsity of vector $\Delta \boldsymbol{\alpha}(\lambda)$.

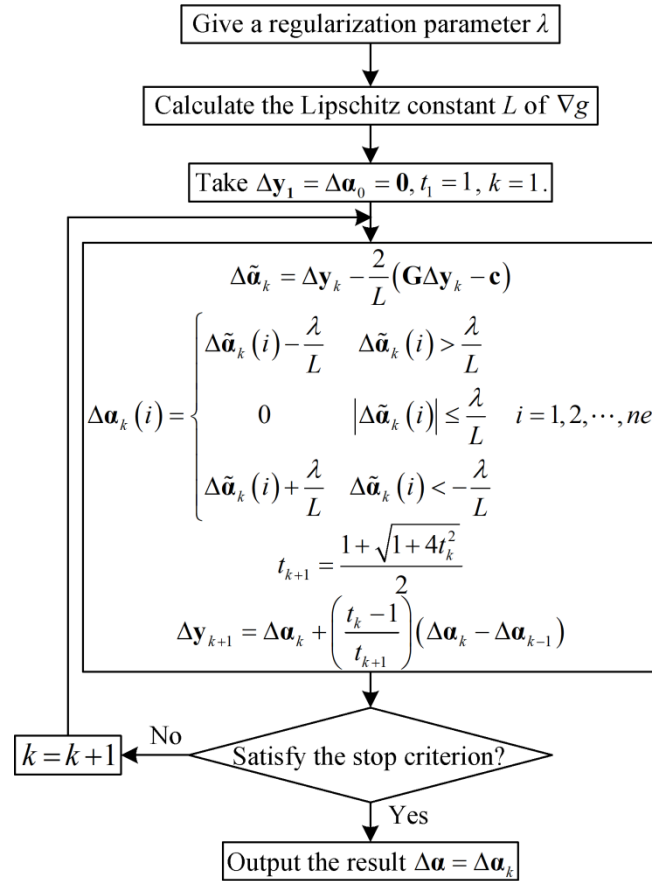


Fig. 4 FISTA to solve Eq. (16) with constant step size

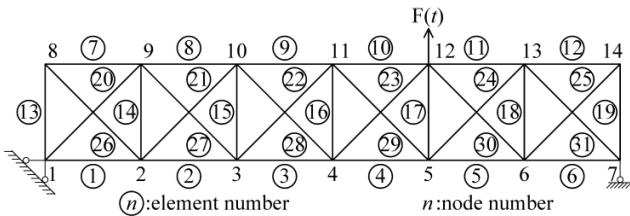


Fig. 5 Geometric configuration of 31-bar planar truss

3. Numerical simulations

To validate the effectiveness and feasibility of the proposed method, some numerical simulations in a 31-bar planar truss, as shown in Fig. 5, are conducted in this study.

The sectional dimension of each bar is $b \times h = 0.05 \text{ m} \times 0.05 \text{ m}$ with an elastic modulus of 70 GPa and a density of 2770 kg/m³. The bar length is 1.52 m for horizontal and vertical components (Zhang and Xu, 2016). Rayleigh damping is accepted, and the first two damping ratios are assumed to be 1%.

Experimental modal analysis or operational modal analysis can be used to obtain frequencies and mode shapes of the truss. Although both two techniques are available, the inherent uncertainty effects should be considered by using operational modal analysis (Yan and Katafygiotis 2019). Because this study focuses on the effectiveness of the proposed SDD method, experimental modal analysis is adopted here to obtain corresponding frequencies and mode shapes.

The Newmark- β method is used to calculate structural acceleration responses. The maximum frequency of the structure is 1040.24 Hz, so the sampling frequency is set as 32768 Hz to obtain sufficiently accurate acceleration responses. The duration time is 8 s, and a logarithmic chirp is applied on the vertical direction of node 12 from 1 s to 5 s. The instantaneous frequency is 0.1 Hz initially and 1100 Hz at the end.

White noises are respectively added into each calculated acceleration response as the measurement noises (Liu *et al.* 2020):

$$\mathbf{r}^n = \mathbf{r} + lev \times \frac{1}{N} \sum_{j=1}^N |\mathbf{r}_j| \times \mathbf{randn} \quad (20)$$

where, \mathbf{r} and \mathbf{r}^n are the noise-free and noisy responses, respectively, lev is the noise level, N is the element number in the vector \mathbf{r} , \mathbf{randn} is a vector drawn from the standard normal distribution.

Herein, the noise level is considered as $lev = 0.05$. Three damaged states are considered in the planar truss, which can be seen in Table 1. Moreover, vertical mode shapes of nodes 9-13 are used for SDD. The corresponding SDD results obtained by the proposed method can be seen in Table 2.

The damaged state with multiple damages in Table 1 is taken as an example to illustrate the proposed method in detail. The noisy force and typical acceleration response are respectively shown in Figs. 6-7.

Table 1 Different damaged states of planar truss

State numbers	Identified damaged states stiffness loss (element)		
Single damage	15% (Element 3)		
Two damages	10% (Element 3)	15% (Element 20)	
Multiple damages	10% (Element 3)	5% (Element 10)	15% (Element 20)

Table 2 SDD results of given damaged states

State numbers	Identified damaged states stiffness loss (element)		
Single damage	15.58% (Element 3)		
Two damages	9.67% (Element 3)	14.80% (Element 20)	
Multiple damages	8.79% (Element 3)	4.73% (Element 10)	15.89% (Element 20)

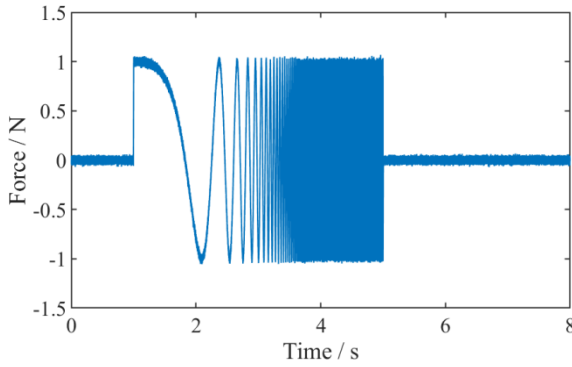


Fig. 6 Noisy force on vertical direction of node 12

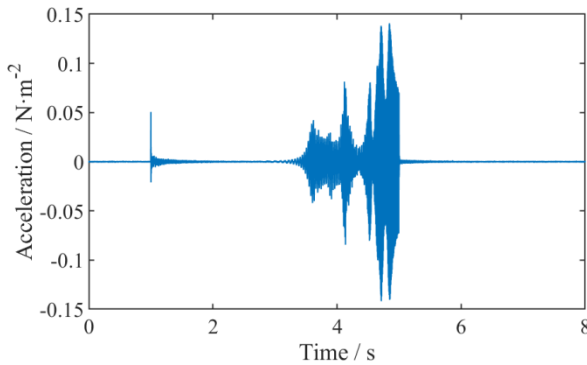


Fig. 7 Noisy acceleration response on vertical direction of node 12

The average number for measured FRFs is 10. As a result, the stabilization diagram is given in Fig. 8. Based on Fig. 8, the first three modes are selected for SDD due to their good robustness. The mode order is selected as 12. Thus, the first three frequencies and mode shapes are calculated from acceleration responses. Moreover, the weight coefficient γ is selected according to Fig. 9.

The weighted coefficient γ greatly affects the SDD results because it balances the contributions between the

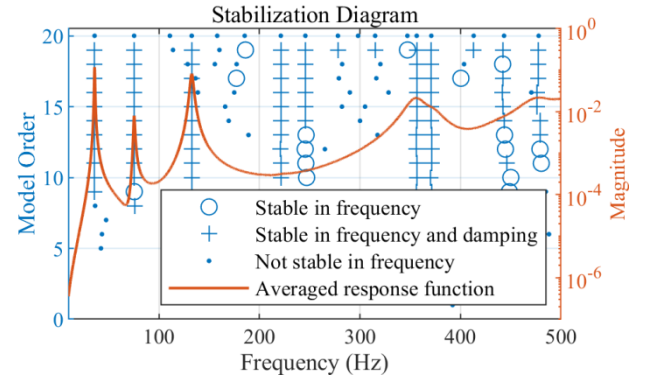


Fig. 8 Stabilization diagram of given FRFs

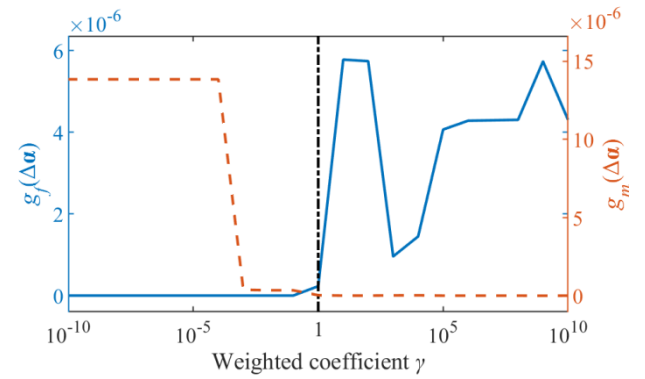


Fig. 9 Guided curves for selecting weighted coefficient

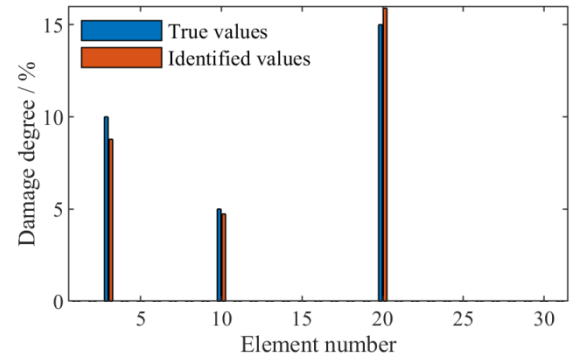


Fig. 10 SDD result for multiple damages in 31-bar planar truss

residual errors $g_f(\Delta\alpha)$ in Eq. (13) and $g_m(\Delta\alpha)$ in Eq. (11) (Cha and Buyukozturk 2015). From Fig. 9, it can be seen that both frequencies and mode shapes are influenced by the measurement noises. When the weighted coefficient is suitable, the residual errors of both $g_f(\Delta\alpha)$ and $g_m(\Delta\alpha)$ will decrease. Therefore, the weighted coefficient γ is chosen as 1 for the given multiple damages. As a result, the SDD result is shown in Fig. 10.

Moreover, the selected near-optimal regularization parameters and weighted coefficients for the given damaged states are given in Table 3.

From the SDD results, it can be seen that the proposed method can effectively identify the given structural damages with high accuracy. Under the influences of noises, the identified damage degrees are smaller or larger

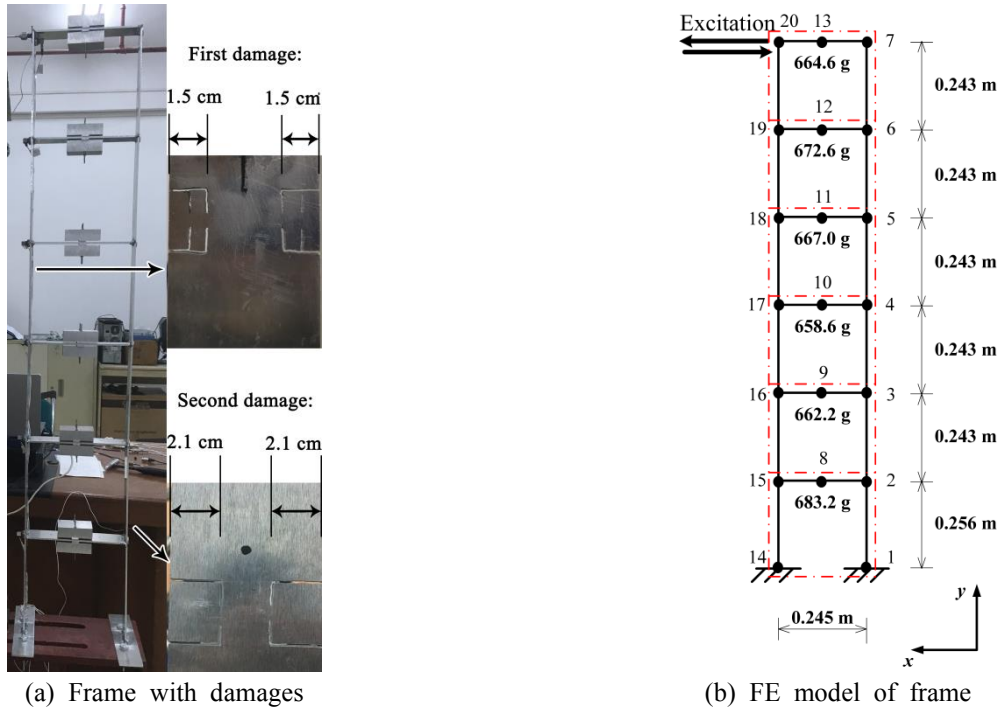


Fig. 11 Six-story aluminum alloy frame in laboratory

Table 3 Regularization parameter and weighted coefficient

State numbers	Regularization parameter λ_{opt}	Weighted coefficient γ
Single damage	2.4133×10^{-5}	1×10^2
Two damages	1.6421×10^{-7}	0.01
Multiple damages	1.8020×10^{-6}	1

than the given damage values. However, the identified damage degrees are approximate to the true values. It indicates that the given ways to select the regularization parameter λ_{opt} and the weighted coefficient γ are reasonable. Moreover, the sparse regularization is suitable for SDD because sparse solutions can be obtained.

4. Experimental verifications

4.1 Experimental setup

To further evaluate the effectiveness of the proposed method, a six-story aluminum alloy frame is designed and fabricated in laboratory. Two structural damages are considered in the columns of frame. The first structural damage is cut on the fourth floor of frame, and the second structural damage is further cut on the second floor of frame, as shown in Fig. 11(a). The cut heights of these two damages are 2.48×10^{-2} m, and the cut widths can be seen in Fig. 11(a). Thus, only changes in the stiffness are considered for SDD. As a result, two damaged states are detected in the frame. The thickness of both columns and beams are 0.004 m.

A diagram of a 20-node FE model for frame can be seen in Fig. 11(b). Six masses are respectively added in the x and

y directions of nodes 8-13, and a periodic chirp is applied in the x direction of node 20. The instantaneous frequency is 0.001 Hz initially and 128 Hz at the end. The sampling frequency is 256 Hz, and the duration is 16 s.

As shown in Fig. 11(b), the elements in each floor are grouped as a super-element. Therefore, for this six-story frame, six super-elements are obtained. Then, because only six accelerometers are placed at nodes 15-20, to effectively detect damages, the DOFs at x direction of nodes 15-20 are selected as the master DOFs, the corresponding numbers of master DOFs are given as 1-6. Other DOFs are selected as the slave DOFs. As a result, a six-DOF reduced model is obtained for SDD by using the System Equivalent Expansion Reduction Process (SEREP) model reduction method (O'Callahan 1989, Koutsovasilis and Beitelshmidt, 2007), and the reduced model is used to describe the frame in healthy state.

The global stiffness and mass matrices of the reduced model are respectively calculated as follows:

$$\mathbf{K}_r = \mathbf{T}^T \mathbf{K} \mathbf{T} \quad (21)$$

$$\mathbf{M}_r = \mathbf{T}^T \mathbf{M} \mathbf{T} \quad (22)$$

with the transformation matrix:

$$\mathbf{T} = \begin{Bmatrix} \Phi_m \\ \Phi_s \end{Bmatrix} (\Phi_m^T \Phi_m)^{-1} \Phi_m^T \quad (23)$$

where, \mathbf{K}_r and \mathbf{M}_r are global stiffness and mass matrices of the reduced model, Φ_m and Φ_s are modal matrices related to master and slave DOFs, respectively.

Moreover, for the super-element in the i th floor, its stiffness matrix is represented by $\mathbf{K}_i^{\text{super}}$, and it is also reduced by the transformation matrix:

Table 4 First six modal parameters for frame and reduced model

Modes	Frequencies		Mode Shapes
	Frame	Reduced model	MAC
1	4.43 Hz	4.35 Hz	0.9997
2	13.45 Hz	13.61 Hz	0.9985
3	24.18 Hz	24.20 Hz	0.9971
4	36.33 Hz	36.32 Hz	0.9960
5	49.13 Hz	49.04 Hz	0.9981
6	59.83 Hz	59.87 Hz	0.9995

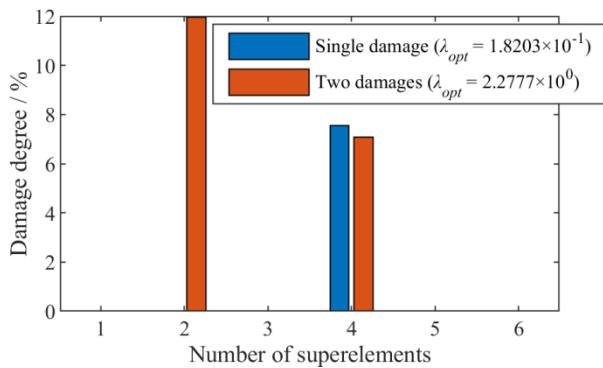


Fig. 12 SDD results of given structural damages in six-story frame

$$\mathbf{K}_{r(i)}^{super} = \mathbf{T}^T \mathbf{K}_i^{super} \mathbf{T} \quad (24)$$

These matrices will be used for SDD in the reduced model. By considering the error caused by model reduction method and model fabrication, in this paper, some parameters are modified according to the ideal parameters. The elastic modulus and density of frame are 72.15 GPa and 2835 kg/m³, respectively. Widths of columns and beams are 6.30×10⁻² m and 5.78×10⁻² m, respectively. Moreover, the height of each floor can be seen in Fig. 11(b).

As a result, the first six modal parameters of both reduced model and frame are compared in Table 4, which indicates the modal parameters obtained from the reduced model are approximate to measured values.

The first six frequencies and mode shapes are used for SDD. By using the proposed method, the SDD results in the given structural damages can be seen in Fig. 12.

Meanwhile, the weighted coefficients are respectively selected for these two damaged states according to Figs. 13 and 14.

As mentioned above, the cut heights of these two damages are the same, and the cut widths in the second and fourth floors are 4.2 cm and 3.0 cm, respectively. Under the influence of structural damages, the reduced moments of inertia in the second and fourth floors are 2.24×10⁻¹⁰ m⁴ and 1.60×10⁻¹⁰ m⁴, respectively. Thus, the residual moments of inertia in these sections are respectively 1.12×10⁻¹⁰ m⁴ and 1.76×10⁻¹⁰ m⁴ for the second and fourth floors. Thus, the ratio of residual moments of inertia in the second and fourth floors is (1.12×10⁻¹⁰)/(1.76×10⁻¹⁰)×100% = 63.64% .

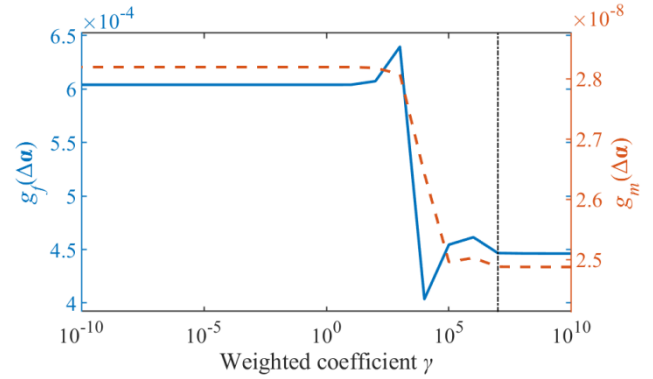


Fig. 13 Guided curves to select weighted coefficient for given single damage

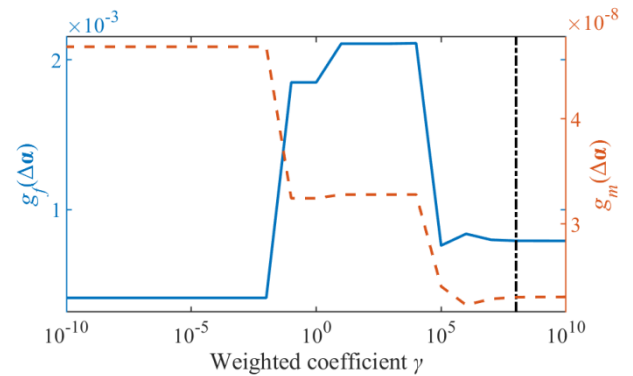


Fig. 14 Guided curves to select weighted coefficient for given two damages

On the other hand, for the given two damages, from Fig. 12, it can be found that the identified damage degrees in the second and fourth super-elements are 11.96% and 7.09%, respectively. Thus, the ratio of damage coefficients in this damaged state for these two super-elements is (1-0.1196)/(1-0.0709)×100% = 59.28%, which is approximate to the ratio of effective residual moments of inertia in the corresponding floors. It shows that the damage degree in the second floor is larger than that in the fourth floor for both the FE model and the frame.

However, as mentioned above, the elements in each floor are grouped as a super-element, and the changes of stiffness in these super-elements are used to describe structural damages. The structural damages only occur in the partial positions of the second and fourth floors, as shown in Fig. 11. Therefore, although the ratios of residual moments of inertia and damage coefficients are close, they cannot accurately reflect damage degrees in the frame. The internal relationship between the equivalent damage degrees in the FE model and the true damage degrees in the frame will be further studied in the future.

Moreover, for these two damaged states, the identified damage degrees of the super-element in the fourth floor are 7.55% and 7.09%, respectively. The identified damage degrees for these two damaged states are close. It indicates that the SDD results accord with the known conditions. Therefore, it shows that the proposed method can effectively detect structural damages in the frame.

From Figs. 13 and 14, it shows that the weighted coefficients greatly affect the residual errors $g_r(\Delta\alpha)$ in Eq. (13) and $g_m(\Delta\alpha)$ in Eq. (11) in different extents. Frequencies and mode shapes are influenced by noises, and they can reflect structural damages in different perspectives. Because the SDD results are reasonable, it indicates that the multi-strategy SDD method proposed in this study has a good robustness to noise.

5. Conclusions

Based on the included angle of vectors and sparse regularization, a multi-strategy structural damage detection (SDD) method is proposed in this paper. Firstly, rather than the difference of vectors, the included angle of vectors is adopted to establish a relationship between mode shapes and changes in damage coefficients. Then, frequencies are introduced for multi-strategy SDD with mode shapes by using a weighted coefficient. Meanwhile, to improve the accuracy of SDD results, sparse regularization is introduced by considered the sparsity of structural damages. As a result, a novel convex optimization problem is defined for effective SDD. To evaluate the effectiveness of the proposed method, numerical simulations in a planar truss and experimental studies in a six-story aluminum alloy frame are conducted. Based on the SDD results, some conclusions are made as follows:

- The proposed multi-strategy SDD method can effectively locate structural damages and quantify damage degrees with a high robustness to noise.
- It is reasonable to simultaneously use both frequencies and mode shapes for SDD because they can reflect structural damages in different perspectives.
- It is effective to select the near-optimal regularization parameter and weighted coefficient by the given ways, and accurate SDD results can be obtained.
- Approximate relationships between modal parameters and damage coefficients are used for SDD, the influence of these relationships will be further studied to improve the identified accuracy in the future.

Acknowledgments

The project is jointly supported by the National Natural Science Foundation of China with Grant Numbers 51678278 and 51278226.

References

Alkayem, N.F., Cao, M., Zhang, Y., Bayat, M. and Su, Z. (2018), "Structural damage detection using finite element model updating with evolutionary algorithms: a survey", *Neural Comput. Appl.*, **30**(2), 389-411. <https://doi.org/10.1007/s00521-017-3284-1>.

Allemang, R.J. (2003), "The modal assurance criterion - Twenty years of use and abuse", *Sound Vib.*, **37**(8), 14-23.

Bagherahmadi, S.A. and Seyedpoor, S.M. (2018), "Structural

damage detection using a damage probability index based on frequency response function and strain energy concept", *Struct. Eng. Mech.*, **67**(4), 327-336. <https://doi.org/10.12989/sem.2018.67.4.327>.

Beck, A. and Teboulle, M. (2009), "A fast iterative shrinkage-thresholding algorithm for linear inverse problems", *SIAM J. Imaging Sci.*, **2**(1), 183-202. <https://doi.org/10.1137/080716542>.

Cawley, P. and Adams, R.D. (1979), "The location of defects in structures from measurements of natural frequencies", *J. Strain Anal. Eng. Des.*, **14**(2), 49-57. <https://doi.org/10.1243/03093247V142049>.

Cha, Y.J. and Buyukozturk, O. (2015), "Structural damage detection using modal strain energy and hybrid multiobjective optimization", *Comput.-Aided Civ. Inf.*, **30**(5), 347-358. <https://doi.org/10.1111/mice.12122>.

Chang, M., Kim, J.K. and Lee, J. (2019), "Hierarchical neural network for damage detection using modal parameters", *Struct. Eng. Mech.*, **70**(4), 457-466. <https://doi.org/10.12989/sem.2019.70.4.457>.

Esfandiari, A., Chaei, M.G. and Rofooei, F.R. (2018), "A structural model updating method using incomplete power spectral density function and modal data", *Struct. Eng. Mech.*, **68**(1), 39-51. <https://doi.org/10.12989/sem.2018.68.1.039>.

Fan, W. and Qiao, P. (2011), "Vibration-based damage identification methods: A review and comparative study", *Struct. Hlth. Monit.*, **10**(1), 83-111. <https://doi.org/10.1177/1475921710365419>.

Friswell, M.I. (2007), "Damage identification using inverse methods", *Philos. T. R. Soc. A*, **365**(1851), 393-410. <https://doi.org/10.1098/rsta.2006.1930>.

Hou, R., Xia, Y. and Zhou, X. (2018), "Structural damage detection based on l_1 regularization using natural frequencies and mode shapes", *Struct. Control Hlth. Monit.*, **25**, e2107. <https://doi.org/10.1002/stc.2107>.

Huang, Q., Xu, Y.L., Li, J.C., Su, Z.Q. and Liu, H.J. (2012), "Structural damage detection of controlled building structures using frequency response functions", *J. Sound Vib.*, **331**(15), 3476-3492. <https://doi.org/10.1016/j.jsv.2012.03.001>.

Koutsovasilis, P. and Beitelschmidt, M. (2007), "Model reduction comparison for the elastic crankshaft mechanism". *Proceedings of the 2nd International Operational Modal Analysis Conference*, Copenhagen, Denmark, April.

Lee, U. and Shin, J. (2002), "A frequency response function-based structural damage identification method", *Comput. Struct.*, **80**(2), 117-132. [https://doi.org/10.1016/S0045-7949\(01\)00170-5](https://doi.org/10.1016/S0045-7949(01)00170-5).

Li, X.Y., Wang, L.X., Law, S.S. and Nie, Z.H. (2017), "Covariance of dynamic strain responses for structural damage detection", *Mech. Syst. Signal Pr.*, **95**, 90-105. <https://doi.org/10.1016/j.ymssp.2017.03.020>.

Li, Y. and Chen, Y. (2013), "A review on recent development of vibration-based structural robust damage detection", *Struct. Eng. Mech.*, **45**(2), 159-168. <https://doi.org/10.12989/sem.2013.45.2.159>.

Liddle, A.R. (2007), "Information criteria for astrophysical model selection", *Mon. Not. R. Astron. Soc.*, **377**(1), L74-L78. <https://doi.org/10.1111/j.1745-3933.2007.00306.x>.

Liu, H.L., Yu, L., Luo, Z.W. and Pan, C.D. (2020) "Compressed sensing for moving force identification using redundant dictionaries", *Mech. Syst. Signal Pr.*, **138**, 106535. <https://doi.org/10.1016/j.ymssp.2019.106535>.

Liu, L., Hua, W. and Lei, Y. (2018), "Real-time simultaneous identification of structural systems and unknown inputs without collocated acceleration measurements based on MEKF-UI", *Measurement*, **122**, 545-553. <https://doi.org/10.1016/j.measurement.2017.07.001>.

Moughty, J.J. and Casas, J.R. (2017), "A state of the art review of modal-based damage detection in bridges: development,

- challenges, and solutions”, *Appl. Sci.*, **7**(5), 510. <https://doi.org/10.3390/app7050510>.
- O’Callahan, J. (1989), “System equivalent reduction expansion process (SEREP)”. *Proceedings of the 7th International Modal Analysis Conference*, Las Vegas, U.S.A., February.
- Pandey, A.K., Biswas, M. and Samman, M.M. (1991), “Damage detection from changes in curvature mode shapes”, *J. Sound Vib.*, **145**(2), 321-332. [https://doi.org/10.1016/0022-460X\(91\)90595-B](https://doi.org/10.1016/0022-460X(91)90595-B).
- Ratcliffe, C.P., (1997), “Damage detection using a modified laplacian operator on mode shape data”, *J. Sound Vib.*, **204**(3), 505-517. <https://doi.org/10.1006/jsvi.1997.0961>.
- Shi, Z.Y., Law, S.S. and Zhang, L.M. (1998), “Structural damage localization from modal strain energy change”, *J. Sound Vib.*, **218**(5), 825-844. <https://doi.org/10.1006/jsvi.1998.1878>.
- Vahidi, M., Vahdani, S., Rahimian, M., Jamshidi, N. and Kanee, A.T. (2019), “Evolutionary-base finite element model updating and damage detection using modal testing results”, *Struct. Eng. Mech.*, **70**(3), 339-350. <https://doi.org/10.12989/sem.2019.70.3.339>.
- Yan, W.J. and Katafygiotis, L.S. (2019), “An analytical investigation into the propagation properties of uncertainty in a two-stage fast Bayesian spectral density approach for ambient modal analysis”, *Mech. Syst. Signal Pr.*, **118**, 503-533. <https://doi.org/10.1016/j.ymssp.2018.08.047>.
- Yan, W.J., Zhao, M.Y., Sun, Q. and Ren, W.X. (2019), “Transmissibility-based system identification for structural health monitoring: Fundamentals, approaches, and applications”, *Mech. Syst. Signal Pr.*, **117**, 453-482. <https://doi.org/10.1016/j.ymssp.2018.06.053>.
- Yan, Y.J., Cheng, L., Wu, Z.Y. and Yam, L.H. (2007), “Development in vibration-based structural damage detection technique”, *Mech. Syst. Signal Pr.*, **21**(5), 2198-2211. <https://doi.org/10.1016/j.ymssp.2006.10.002>.
- Zhang, C.D. and Xu, Y.L. (2016), “Comparative studies on damage identification with Tikhonov regularization and sparse regularization”, *Struct. Control Hlth. Monit.*, **23**(3), 560-579. <https://doi.org/10.1002/stc.1785>.
- Zhao, J. and DeWolf, J.T. (1999), “Sensitivity study for vibrational parameters used in damage detection”, *J. Struct. Eng.*, **125**(4), 410-416. [https://doi.org/10.1061/\(ASCE\)0733-9445\(1999\)125:4\(410\)](https://doi.org/10.1061/(ASCE)0733-9445(1999)125:4(410)).
- Zhou, X.Q., Xia, Y. and Weng, S. (2015), “L₁ regularization approach to structural damage detection using frequency data”, *Struct. Hlth. Monit.*, **14**(6), 571-582. <https://doi.org/10.1177/1475921715604386>.
- Zhou, Y.L. and Wahab, M.A. (2017), “Cosine based and extended transmissibility damage indicators for structural damage detection”, *Eng. Struct.*, **141**, 175-183. <https://doi.org/10.1016/j.engstruct.2017.03.030>.